Atypical α-Conotoxin LtIA from *Conus litteratus* Targets a Novel Microsite of the α3β2 Nicotinic Receptor*

Sulan Luo[‡1], Kalyana Bharati Akondi[§], Dongting Zhangsun[‡], Yong Wu[‡], Xiaopeng Zhu[‡], Yuanyan Hu[‡], Sean Christensen[¶], Cheryl Dowell[¶], Norelle L. Daly[§], David J. Craik[§], Ching-I Anderson Wang[§], Richard J. Lewis[§], Paul F. Alewood[§], and J. Michael McIntosh[¶]

From the ‡Key Laboratory of Tropical Biological Resources, Ministry of Education, Ocean College, College of Materials and Chemical Engineering, Center for Experimental Biotechnology, Hainan University, Haikou Hainan 570228, China, the §Institute for Molecular Bioscience and School of Biomedical Sciences, University of Queensland, Brisbane, Queensland 4072, Australia, and the ¶Departments of Biology and Psychiatry, University of Utah, Salt Lake City, Utah 84112

Different nicotinic acetylcholine receptor (nAChR) subtypes are implicated in learning, pain sensation, and disease states, including Parkinson disease and nicotine addiction. α-Conotoxins are among the most selective nAChR ligands. Mechanistic insights into the structure, function, and receptor interaction of α-conotoxins may serve as a platform for development of new therapies. Previously characterized α-conotoxins have a highly conserved Ser-Xaa-Pro motif that is crucial for potent nAChR interaction. This study characterized the novel α-conotoxin LtIA, which lacks this highly conserved motif but potently blocked α3β2 nAChRs with a 9.8 nM IC_{50} value. The off-rate of LtIA was rapid relative to Ser-Xaa-Pro-containing α-conotoxin MII. Nevertheless, pre-block of α3β2 nAChRs with LtIA prevented the slowly reversible block associated with MII, suggesting overlap in their binding sites. nAChR β subunit ligand-binding interface mutations were used to examine the >1000-fold selectivity difference of LtIA for α3β2 *versus* α3β4 nAChRs. Unlike MII, LtIA had a >900-fold increased IC_{50} value on α3β2(F119Q) *versus* wild type nAChRs, whereas T59K and V111I β2 mutants had little effect. Molecular docking simulations suggested that LtIA had a surprisingly shallow binding site on the α3β2 nAChR that includes β2 Lys-79. The K79A mutant disrupted LtIA binding but was without effect on an LtIA analog where the Ser-Xaa-Pro motif is present, consistent with distinct binding modes.

Neuronal nAChRs[2] are found throughout the central and peripheral nervous system. These nAChRs, located both pre-

and post-synaptically, modulate the release of neurotransmitters and/or mediate fast synaptic transmission (1, 2). In addition, nAChRs are present in a variety of non-neuronal tissue, including epithelium and immune cells. In mammals, there are nine α and four β nAChR subunits that can combine to form multiple subtypes of hetero-pentamers (3). The array of physiological functions mediated by nAChRs is correspondingly broad. Compounds acting on nicotinic receptors are currently utilized as medications for treating nicotine addiction and are being explored as therapeutic options for a variety of conditions, including cognitive disorders and pain (4). Understanding the factors contributing to ligand-nAChR subtype specificity will play a crucial role in developing compounds that have the desired therapeutic effects but that lack side effects (5).

Many phyla utilize acetylcholine for neurotransmission. Predatory organisms have exploited this by developing toxins that act at nAChRs to disrupt the flight and fight of their prey (6). Predatory marine snails of the genus *Conus* synthesize complex venoms that contain an arsenal of peptides. Over the past several years, these "conotoxins" have been shown to have a remarkable diversity of pharmacological function and utility (7, 8). Based on molecular structure, the conotoxins have been grouped into A, O, M, P, R, S, and T superfamilies (9, 10). A subgroup of compounds found within the A superfamily is the α-conotoxins. These are small, 13–21-residue, cysteine-rich peptides that functionally block nAChRs (11, 12). Structural studies utilizing NMR spectroscopy and x-ray crystallography have provided insight into the role and spatial location of residues important for function (13).

Previously characterized α-conotoxins have a highly conserved Ser-Xaa-Pro motif in the first intercysteine loop. The Pro residue is essential for high affinity binding to nAChRs (14). This study characterizes the novel α4/7 conotoxin LtIA, which lacks the highly conserved Ser-Xaa-Pro sequence but maintains high potency. (The 4/7 terminology refers to the number of non-Cys residues in the first and second intercysteine loops present in all α-conotoxins.) Structural and functional studies provide insight into the mechanism of action and the nature of the nAChR-binding site of LtIA. nAChRs are pentamers made

[1] To whom correspondence should be addressed: Key Laboratory of Tropical Biological Resources, Ministry of Education, Center for Experimental Biotechnology, Hainan University, Haikou Hainan 570228 China. Fax: 86-898-66276720; E-mail: luosulan2003@163.com.

[2] The abbreviations used are: nAChR, nicotinic acetylcholine receptor; AChBP, acetylcholine-binding protein; CTX, conotoxin; HPLC, high pressure liquid chromatography; ACh, acetylcholine; PDB, Protein Data Bank; Fmoc, *N*-(9-fluorenyl)methoxycarbonyl; ESI-MS, electrospray ionization-mass spectrometry; NOESY, nuclear Overhauser effect spectroscopy.

up of α and β subunits. Previous reports indicated that the ACh-binding site is composed of a hydrophobic group of conserved aromatic residues from both the α and β subunits in proximity to the two disulfide-linked vicinal cysteines of the α subunit C loop. High conservation of residues that form the ligand-binding interface among subtypes of nAChRs hinders the ability of ligands to discriminate among these subtypes. However, nonconserved residues appear to line a binding cleft, and functional understanding of these residues could be utilized to develop subtype-specific ligands (15, 16). Mutation of one of these residues, nAChR β2 subunit Phe-119, substantially reduces the block by LtIA. This decrease in activity is the largest effect described thus far for a β subunit mutant affecting α-conotoxin block and was supported by molecular docking simulations. α-Conotoxin LtIA, the first α-conotoxin to be identified from *Conus litteratus* of the South China Sea, provides a novel probe of nAChR structure and function. This study suggests there is a novel, shallow microsite for α-conotoxins lacking the conserved Ser-Xaa-Pro motif.

EXPERIMENTAL PROCEDURES

Materials—Acetylcholine chloride, atropine, and bovine serum albumin were obtained from Sigma. Reversed-phase HPLC analytical Vydac C18 column (5 μm, 4.6 × 250 mm) and preparative C18 Vydac column (10 μm, 22 × 250 mm) were obtained from Shenyue (Shanghai City, China). Reagents for peptide synthesis were from Applied Biosystems (Guangzhou City, China). Acetonitrile was purchased from Fisher. Trifluoroacetic acid was from Tedia Co. (Fairfield, OH). All other chemicals used were of analytical grade. The sequence of α-conotoxin LtIA (GCCARAACAGIHQELC) was based on a cDNA clone (LeD2P) from *C. litteratus* from Hainan, China (Table 1) (17). A highly similar cDNA sequence was also reported from *Conus leopardus* (18). Clones of rat α2–α7 and β2–β4 as well as mouse muscle α1β1δε cDNAs were kindly provided by S. Heinemann (Salk Institute, San Diego). Clones of β2 and β3 subunits in the high expressing pGEMHE vector were kindly provided by C. W. Luetje, University of Miami, Miami, FL).

Peptide Synthesis by One-step Oxidation—α-Conotoxin LtIA was assembled by solid-phase methodology on an ABI 433A peptide synthesizer using FastMoc chemistry and standard side chain protection. All cysteines were protected with *S*-trityl groups. The peptides were removed from a solid support by treatment with reagent K (trifluoroacetic acid/water/ethanedithiol/phenol/thioanisole, 82.5:5:2.5:5:5, v/v). The released peptide was precipitated and washed several times with cold ether. The reduced peptides were purified by reverse-phase HPLC using a preparative C18 Vydac column with a linear gradient of acetonitrile in 0.1% (v/v) trifluoroacetic acid. The flow rate was 10 ml/min, and elution was monitored by UV detection at 215 nm. Identity of each peptide was confirmed by ESI-MS analysis. After purification, the linear peptide was lyophilized. Folding was carried out in a buffered solution of 0.1 M NH_4HCO_3, pH 7.5, containing 1 mM EDTA. The final peptide concentration was 20 μM. The reaction was allowed to proceed at room temperature (25 °C) for 72 h. The reaction mixture was then quenched by acidification with formic acid (8% final concentra-

tion), and the samples were separated by analytical reverse-phase C18 HPLC, using the following gradient of acetonitrile at a flow rate of 1 ml/min: 0–50 min 0–50% solvent B, 50–55 min 50–100% solvent B. Solvent B is 0.05% trifluoroacetic acid in 90% acetonitrile.

The analogs LtIA(A4S/A6P) and LtIA(A4S) were manually synthesized by *t*-butoxycarbonyl chemistry coupled with *in situ* neutralization protocol on 4-methylbenzhydrylamine amide resin (Peptide Institute). 0.5 M 2-(1*H*-benzotriazole-1-yl)-1,1,3,3-tetramethyluronium hexafluorophosphate in *N*,*N*-dimethylformamide was the activation agent; diisopropylethylamine was the neutralization agent, and the terminal amide protection groups were removed using trifluoroacetic acid. The peptides were cleaved off the resin using HF with *p*-cresol and *p*-thiocresol as scavengers (HF/*p*-cresol/*p*-thiocresol, 10:1:1, v/v) at 0 °C for 1 h. The peptides were then precipitated with cold diethyl ether, dissolved in 50% acetonitrile containing 0.05% trifluoroacetic acid, and lyophilized. The mass of the crude peptides was verified by ESI-MS on Applied Biosystems API 2000 liquid chromatography/mass spectrometry. The crude peptides were purified by preparative reverse-phase HPLC using a Vydac C18 column (22 × 250 mm, 10 μm) on a Waters 600E solvent delivery system using a linear gradient of 1% buffer B per min at a flow rate of 10 ml/min (buffer A, H_2O, 0.05% trifluoroacetic acid; buffer B, 90% acetonitrile, 10% H_2O, 0.043% trifluoroacetic acid), and the eluant was monitored at 230 nm.

Disulfide bonds were formed by air oxidation of free thiol groups on cysteine residues in 0.1 M NH_4HCO_3 buffer with 30% isopropyl alcohol. The reaction was carried out overnight at room temperature, and the peptide concentration was 0.1 mg/ml. The molecular weight of the folded peptide was verified by ESI-MS, which was then purified and lyophilized. The purity of the product obtained after each purification step was determined by analytical reverse-phase HPLC using Shimadzu LC-2010 system using a Vydac C18 column (4.6 × 250 mm, 5 μm) at the flow rate of 1 ml/min.

Peptide Synthesis by Two-step Oxidation—α-Conotoxin LtIA was synthesized on an amide resin using Fmoc chemistry and standard side protection, except for cysteine residues. Cys residues were protected in pairs with either *S*-trityl on Cys-2 and Cys-8 or *S*-acetamidomethyl on Cys-3 and Cys-16. The crude peptide was cleaved from the resin and precipitated. A two-step oxidation protocol was used to fold the peptides selectively as described previously (19). Briefly, the disulfide bridge between Cys-2 and Cys-8 was closed by dripping the peptide into an equal volume of 20 mM potassium ferricyanide, 0.1 M Tris, pH 7.5. The solution was allowed to react for 30 min, and the monocyclic peptide was purified by reverse-phase HPLC. Simultaneous removal of the *S*-acetamidomethyl groups and closure of the disulfide bridge between Cys-3 and Cys-16 were carried out by iodine oxidation as follow; the monocyclic peptide in HPLC eluent was dripped into an equal volume of iodine (10 mM) in H_2O/trifluoroacetic acid/acetonitrile (78:2:20 by volume) and allowed to react for 10 min. The reaction was terminated by the addition of ascorbic acid and diluted 20-fold with 0.1% trifluoroacetic acid, and the bicyclic peptide was purified by HPLC on a reverse-phase C18 Vydac column using

a linear gradient of 0.1% and 0.092% trifluoroacetic acid, 60% acetonitrile, and the remainder H_2O. Matrix-assisted laser desorption ionization time-of-flight mass spectrometry was utilized to confirm the identity of the products.

cRNA Preparation and Injection—Capped cRNA for the various subunits were made using the mMessage mMachine *in vitro* transcription kit (Ambion, Austin, TX) following linearization of the plasmid. The cRNA was purified using the Qiagen RNeasy kit (Qiagen, Valencia, CA). The concentration of cRNA was determined by absorbance at 260 nm. cRNA of chimera $α6/α3$ was combined with cRNA of high expressing $β2$ and $β3$ subunits or $β4$ (in the pGEMHE vector) to give 167–500 ng/$μ$l of each subunit cRNA. Fifty nl of this mixture was injected into each *Xenopus* oocyte with a Drummond microdispenser (Drummond Scientific, Broomall, PA), as described previously, and incubated at 17 °C. Oocytes were injected within 1 day of harvesting, and recordings were made 2–4 days post-injection.

Voltage Clamp Recording—Oocytes were voltage-clamped and exposed to ACh and peptide as described previously (20). Briefly, the oocyte chamber consisting of a cylindrical well (~30 $μ$l in volume) was gravity-perfused at a rate of ~2 ml/min with ND-96 buffer (96.0 mM NaCl, 2.0 mM KCl, 1.8 mM $CaCl_2$, 1.0 mM $MgCl_2$, 5 mM HEPES, pH 7.1–7.5) containing 1 $μ$M atropine and 0.1 mg/ml bovine serum albumin. In the case of the $α9α10$ and mouse muscle $α1β1δε$ subtypes, the ND-96 contained no atropine when recording. The oocyte was subjected once a minute to a 1-s pulse of 100 $μ$M ACh. In the case of the $α9α10$ and mouse muscle $α1β1δε$ subtypes, there is a 1-s pulse of 10 $μ$M ACh. 200 $μ$M ACh pulse is for the $α7$ subtype. For screening of receptor subtypes, for toxin concentrations of 10 $μ$M and lower, once a stable base line was achieved, either ND-96 alone or ND-96 containing varying concentrations of the $α$-conotoxins was manually pre-applied for 5 min prior to the addition of the agonist. All recordings were done at room temperature (~22 °C).

Data Analysis—The average of five control responses just preceding a test response was used to normalize the test response to obtain "% response." Each data point of a dose-response curve represents the average ± S.E. of at least four oocytes. The dose-response data were fit to the equation, % response = $100/(1 + ([toxin]/IC_{50})\wedge n_H)$, where n_H is the Hill coefficient, by nonlinear regression analysis using GraphPad Prism (GraphPad Software, San Diego).

Circular Dichroism Analysis—CD spectra were acquired on a Jasco J-810 spectropolarimeter, which was routinely calibrated using 0.6% (w/v) ammonium-*d*-camphor-10-sulfonate. All experiments were conducted at room temperature under a nitrogen atmosphere (15 ml/min). The scanning speed was set to 50 nm/min with response time of 1 s, sensitivity range of 100 millidegrees, and a step resolution of 1 nm. Absorbance was measured in the far-UV region (190–260 nm) using a cell with a 1-mm path length, and each recording was an accumulation of four scans. CD spectra were obtained for peptides dissolved in 20 mM ammonium bicarbonate buffer at pH 7. Spectra were also obtained after addition of 10 and 30% (v/v) trifluoroethanol in phosphate buffer. CD spectra of the pure solvents were subtracted from those of the peptide samples to eliminate interfer-

ence due to solvent, cell, or spectropolarimeter optics. The molar ellipticity [$θ$] was calculated using Equation 1,

$$[θ] = θ/(10 \times C \times Np \times l) \qquad \text{(Eq. 1)}$$

where $θ$ is ellipticity in millidegrees; C is molar concentration of the peptide; Np is number of peptide units ($Np = 15$ for LtIA), and l is the path length of the cell.

NMR Spectroscopy—^{1}H NMR measurements were recorded on a 1 mM solution of the globular isomer of LtIA in 10% D_2O, 90% H_2O at ~pH 3. Spectra were obtained on a Bruker Avance 600-MHz spectrometer at 280, 290, 300, and 310 K. The spectra for LtIA(A4S) and LtIA(A4S/A6P) were recorded at 308 and 290 K, respectively. The two-dimensional NMR experiments consisted of total correlation spectroscopy using an MLEV17 spin lock sequence with an isotropic mixing time of 80 ms and nuclear Overhauser effect spectroscopy (NOESY) experiments with mixing times of 200, 300, and 350 ms. Spectra were recorded in a phase-sensitive mode using time proportional phase incriminations. A modified WATERGATE sequence was used for suppression of the water signal. All spectra obtained were processed using Topspin (Bruker). Resonance assignment was carried out using the program SPARKY.

Molecular Modeling and Docking—Molecular models of rat $α3$ and $β2$ subunits were built individually using $α_1$-nicotinic acetylcholine receptor ($α_1$-nAChR; PDB code 2QC1) (21) as the template, and the interface was created using *Lymnaea stagnalis* acetylcholine-binding protein (Ls-AChBP; PDB code 1IBG) (22) as the template, with the program Modeler 9, version 2 (23). These templates were chosen as they share a high degree of conservation in protein sequence identities with rat $α3$ and $β2$ subunits as determined by BLAST (24).

The native LtIA and its analogs LtIA(A4S) and LtIA(A4S/A6P) vary in their $α$-helical tendencies in solution as suggested by both NMR and CD analyses. Although the bound state of the peptide is unknown, as an initial approach, we built the LtIA, LtIA(A4S) and LtIA(A4S/A6P) models using the TxIA (A10L) template extracted from the *Aplysia californica* AChBP-TxIA(A10L) co-crystal structure (PDB code 2UZ6) (25) All sequence alignments were generated using ClustalW (26) and were further corrected by hand based on the secondary structure alignment to maximize the accuracy of sequence alignment and protein sequence identity. The structural models were validated using the on-line server Verify3D (27) and Ramachandran plot available from ProFunc (28) data base. LtIA, LtIA(A4S), and LtIA(A4S/A6P) and MII (PDB code 1MII) (29, 30) were docked to the $α3β2$ nAChR homology model and Ls-AChBP crystal structure using the program HEX 5.0 (31), and the solutions that disagreed with the known interactions were excluded. The optimal hydrogen bonds between ligands and $α3β2$ nAChR that are likely to contribute to the complex stability were predicted using the on-line server WHAT IF (32).

RESULTS

Chemical Synthesis and Oxidative Folding—$α$-CTX LtIA is a 16-amino acid C-terminally amidated peptide with four Cys residues (Table 1) (17). Fmoc chemistry was used to synthesize the reduced peptide. In the initial synthesis, Cys side chains

α-CTX LtIA, a Novel Structural nAChR Antagonist

Name	Source	Sequence (a)	Target[#]	Ref.
LtIA	*C. litteratus*	GCC**A**RA**A**CAGIHQELC*	α3/β2 >α6/α3β2β3	This work
GIC	*C. geographus*	GCC**S**HP**A**CAGNNQHIC*	α3β2 ~α6/α3β2β3>α4β2 ~α3β4	49
GID	*C. geographus*	IRDγCC**S**NP**A**CRVNNOHVC^	α3β2~α7>α4β2	7
MII	*C. magus*	GCC**S**N**P**VCHLEHSNLC*	α6/β2>α3β2	42
Vc1.1	*C. victoriae*	GCC**S**D**O**RCNYDHPγIC*	α9α10 >α6/α3β2β3>α6/α3β4> α3β4 ~α3β2	50-52 ,
OmIA	*C. omaria*	GCC**S**HP**A**CNVNNPHICG*	α3β2>α7 >α6/α3β2β3	53
PnIA	*C. pennaceus*	GCC**S**L**P**PCAANNPDYC*	α3β2 >α7	54
PnIB	*C. pennaceus*	GCC**S**L**P**PCALSNPDψC*	α7 >α3β2	54
[A10L]-PnIA	*C. pennaceus*	GCC**S**L**P**PCALNNPDψC*	α7>α3β2	55,56
PeIA	*C. pergrandis*	GCC**S**HP**A**CSVNHPELC*	α9α10 >α3β2>α3β24>α7	57
PIA	*C. purpurascens*	RDPCC**S**N**P**VCTVHNPQIC*	α6/α3β2β3 >α3β2 >α3β4	58
AnIB	*C. anemone*	GGCC**S**HPACAANNQDYC*	α3β2>α7	59
EpI	*C. episopatus*	GCC**S**DPRCNMNNPDψC*	α3β2α3β4	60
AuIA	*C. Aulicus*	GCC**S**YPPCFATNSDYC*	α3β4	61
SrIA	*C. spurius*	RTCC**S**R**O**TCRMgYPγLCG*	α4β2, α1β1δγ	62
SrIB	*C. spurius*	RTCC**S**R**O**TCRMEYPγLCG*	α4β2, α1β1δγ	62

(a) O = 4-*trans*-hydroxyproline; γ = γ-carboxyglutamate; ^ = C-terminal carboxylate; ψ = sulfated tyrosine; * = C-terminal carboxamide. The highly conserved Ser and Pro in loop 1 are highlighted in boldface and underlined. The conserved Cys residues are shaded. #, note that all nAChR subtypes were not tested in each instance. Refer to cited literature for full details.

were protected with the acid-labile *S*-trityl group. Cleavage of the peptide from the resin simultaneously removed the *S*-trityl groups. Subsequently, Cys residues were air-oxidized in 1 M NH_4HCO_3, pH 7.5 buffer, containing 1 mM EDTA and purified by HPLC (Fig. 1*A*).

With four Cys residues, there are three possible disulfide bond connectivities. Previously characterized α-conotoxins purified from venom typically have a disulfide bond connectivity linking the 1st Cys to the 3rd Cys and the 2nd Cys to the 4th Cys, which is referred to as the "globular" form to distinguish it from the alternative "ribbon" and "beads" connectivities (33). We therefore also synthesized α-CTX LtIA using a directed two-step folding. Cys pairs as found in native purified peptides were orthogonally protected using acid-labile *S*-trityl and acid-stable *S*-acetamidomethyl groups. Cleavage from the resin selectively removed the *S*-trityl groups, and the deprotected Cys residues were oxidized with potassium ferricyanide. After HPLC purification of the monocyclic peptide, acetamidomethyl groups were removed from the second Cys pair by treatment with iodine that also oxidized the peptide to form the second disulfide bond. The identity of the bicyclic peptide was confirmed by mass spectrometry, average calculated as follows: 1600.66 Da; observed 1600.4 Da. A co-elution experiment was performed with an ~1:1 ratio of the major product of the one-step air oxidation and the major product of the two-step directed oxidation. As shown in Fig. 1*B*, the two products have

identical elution profiles. Thus, the major product of the equilibrium air oxidation folding of the peptide has the disulfide bond configuration of native α-conotoxins. Synthetic peptide with this disulfide bond arrangement was used for all further analysis.

LtIA lacks the conserved Ser-4 and Pro-6 of other α-conotoxins (see Table 1). Accordingly, as part of our study of native LtIA, we also synthesized and characterized one analog in which LtIA Ala-4 was replaced by Ser and another analog in which Ala-4 and Ala-6 of LtIA were replaced by Ser and Pro, respectively. *t*-Butoxycarbonyl chemistry/*in situ* neutralization protocol (34) was used to synthesize the LtIA analogs. Syntheses were carried out on a 0.5 mmol scale with an overall coupling efficiency of >99.7%, as determined by quantitative ninhydrin tests. During assembly, the Cys side chains were protected with HF-labile methylbenzyl groups, which were removed upon cleavage. The reduced peptides were folded in 0.1 M NH_4HCO_3 buffer with 30% isopropyl alcohol, overnight at room temperature. For each analog, ESI-MS analysis showed a decrease in molecular mass by 4 Da, confirming the formation of two disulfide bonds.

Effect of α-CTX LtIA on ACh-evoked Currents through nAChRs—α-Conotoxins have been widely used as pharmacological tools to characterize nAChRs. The effects of α-CTX LtIA on different nAChRs heterologously expressed in *Xenopus* oocytes were analyzed. Fig. 2 shows representative responses to
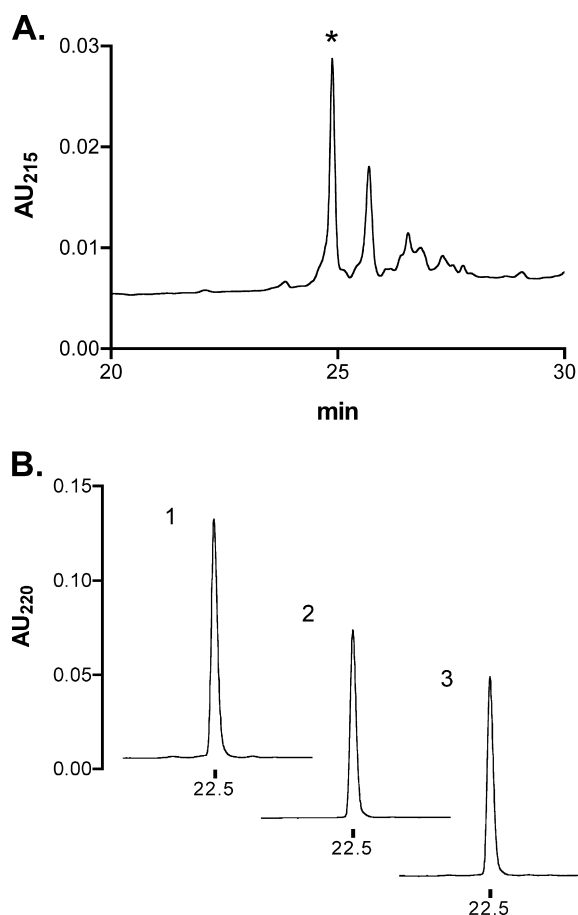
FIGURE 1. **HPLC analysis of the oxidative folding of *α*-CTX LtIA and comparison of the one-step and two-step oxidation methods.** *A*, linear peptide was air-oxidized in one step and purified by analytical HPLC. The *asterisk* denotes the major product that was subjected to co-elution with the two-step oxidation product. *B, 1*, HPLCs of 1 nmol of material from *A*; *2*, ~1 nmol of peptide obtained from the two-step directed folding of the peptide; and *3*, co-elution of 0.5 nmol each of *1* and *2*. Peptides in *B* were analyzed on a reverse-phase analytical Vydac C18 HPLC using a linear gradient of 90% buffer A to 50% buffer B over 40 min, where $A = 0.1\%$ trifluoroacetic acid and $B = 0.92\%$, 60% acetonitrile, remainder water. Absorbance was monitored at 220 nm. *AU*, absorbance units.

ACh of $\alpha3\beta2$, $\alpha4\beta2$, and $\alpha3\beta4$ nAChRs in the presence and absence of α-CTX LtIA. Complete block of ACh-evoked currents was obtained with 1 μM α-CTX LtIA on $\alpha3\beta2$ nAChRs (Fig. 2*A*) compared with little or no block of $\alpha4\beta2$ (Fig. 2*B*) and $\alpha3\beta4$ (Fig. 2*C*) nAChRs by 10 μM LtIA. The block of $\alpha3\beta2$ nAChRs by LtIA is rapidly reversible (Fig. 2*A*). Concentration-response curves for α-CTX LtIA are shown in Fig. 3. $\alpha3\beta2$ nAChRs were most potently blocked by α-CTX LtIA with an IC$_{50}$ of 9.8 nM (Table 2). When a $\beta4$ rather than $\beta2$ nAChR subunit was co-expressed with the $\alpha3$ subunit, the IC$_{50}$ for α-CTX LtIA was >1000-fold higher, thus indicating that amino acid residue differences between the homologous β subunits significantly influence toxin potency. Likewise, LtIA was substantially less potent on $\alpha6/\alpha3\beta4$ *versus* $\alpha6/\alpha3\beta2\beta3$ nAChRs. In contrast, there was little or no block by LtIA at 10 μM LtIA on other nAChR subtypes, including $\alpha1\beta1\delta\epsilon$, $\alpha2\beta2$, $\alpha2\beta4$, $\alpha4\beta2$, $\alpha4\beta4$, $\alpha7$, and $\alpha9\alpha10$, (Table 2).

Block of $\alpha3\beta2$ nAChRs by α-CTX MII Is Prevented by α-CTX LtIA—Where tested, the binding of previously isolated $\alpha4/7$ conotoxins competitively prevents the binding of other nAChR
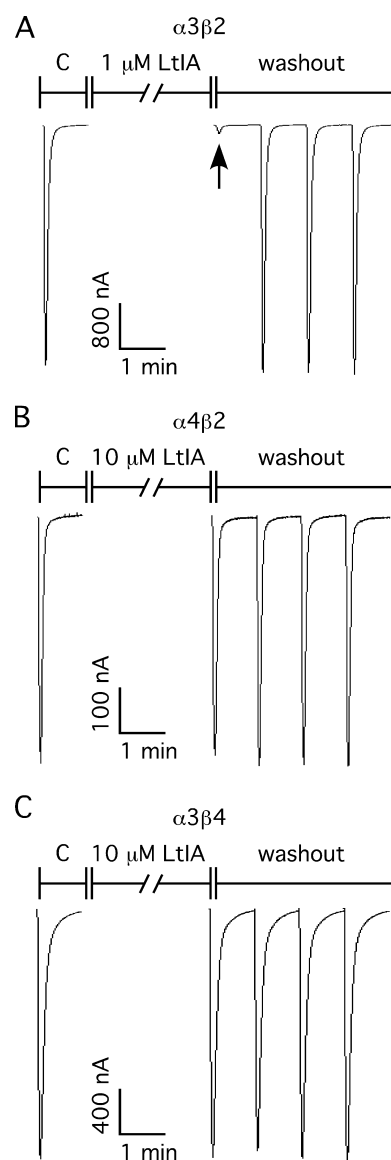

FIGURE 2. **α-CTX LtIA differentially blocks $\alpha3\beta2$ (*A*), $\alpha4\beta2$ (*B*), and $\alpha3\beta4$ (*C*) nAChRs.** Oocytes expressing $\alpha3\beta2$ nAChRs (*A*), $\alpha4\beta2$ nAChRs (*B*), and $\alpha3\beta4$ nAChRs (*C*) were voltage-clamped at -70 mV and subjected to a 1-s pulse of 100 μM ACh every minute as described under "Experimental Procedures." In each panel, the *C* response is control, following which the oocyte was exposed to the peptide for 5 min as indicated under "Experimental Procedures." The 1st trace by the ACh pulse is the peptide response on corresponding nAChRs subtype. *A, arrow* denotes the current response trace of 1 μM LtIA on $\alpha3\beta2$ nAChRs. *B* and *C*, 1st trace after the control is the current response of 10 μM LtIA on $\alpha4\beta2$ and $\alpha3\beta4$ nAChRs, respectively. The ND-96 perfusion and ACh pulses were then resumed to monitor the recovery from block during washout of peptide. The peptide was potent in blocking $\alpha3\beta2$ nAChR and no block on $\alpha4\beta2$ and $\alpha3\beta4$ nAChRs. Likewise, the block of $\alpha3\beta2$ nAChRs was quickly reversible.

agonists and antagonists. In contrast, the $\alpha4/3$ conotoxin ImII is a noncompetitive antagonist. Blocking $\alpha3\beta2$ nAChRs by α-LtIA is rapidly reversible, in contrast to the relatively slow reversibility of α-CTX MII (Fig. 4, *A* and *B*) (35). We utilized this difference in k_{off} values to assess whether LtIA could prevent the binding of the competitive antagonist α-CTX MII. Preapplication of 10 μM LtIA for 1 min prior to application of MII led to a block of $\alpha3\beta2$ nAChRs that was rapidly reversed upon toxin washout, comparable with the reversible block by LtIA
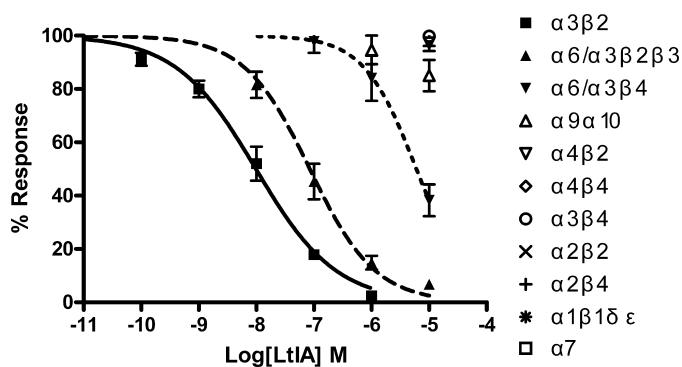
FIGURE 3. **α-CTX LtIA concentration-response on native nAChR subtypes.** Values are means ± S.E. from 5 to 7 separate oocytes. Oocytes expressing 1 of 11 different nAChRs were voltage-clamped and subjected to ACh pulses as described in Fig. 2 and under "Experimental Procedures."

TABLE 2

IC_{50} and Hill slope values for block of various rat nAChR subtypes by α-CTX LtIA

Subtypes	IC_{50}^a	Ratio[b]	Hill slope[a]	Subtypes	IC_{50}^c
	nM				nM
α3β2	9.79 (7.3–13.2)	1	0.63 (0.52–0.73)	α4β4	>10,000
α6/α3β2β3	84.4 (58–123)	8.6	0.76 (0.57–0.96)	α3β4	>10,000
α6/α3β4	5990 (3400–10,500)	612	0.95 (0.43–1.48)	α2β2	>10,000
α9α10	>10,000			α2β4	>10,000
α4β2	>10,000			α1β1δε	>10,000
				α7	>10,000

[a] Numbers in parentheses are 95% confidence intervals.
[b] nAChR subtype $IC_{50}/α3β2\ IC_{50}$ is shown.
[c] No block at 10^{-5} M was seen.

alone. Thus, LtIA is able to prevent the slowly reversible block by MII indicating that LtIA and MII may have overlapping binding sites.

Mutations in the Ligand-binding Site of the β Subunit Affect Blocking by LtIA—LtIA is 3 orders of magnitude more potent on α3β2 *versus* α3β4 nAChRs. Mutations within the nAChR β2 subunit ligand-binding interface were used to determine toxin potency differences for α3β2 *versus* α3β4 nAChRs. Point mutants were constructed in which β4 nAChR residues were substituted for β2 subunit residues that toxin-receptor docking studies have suggested are positioned to interact with α-conotoxins. nAChR β2 mutants T59K, V111I, and F119Q were used to examine the concentration response of α-CTX LtIA (Fig. 5 and Table 3). The toxin had little activity when tested on α3β2 F119Q. In contrast, LtIA potently blocked ACh-evoked currents of α3β2 T59K and V111I nAChRs. The ratios of mutant $IC_{50}/α3β2\ IC_{50}$ were 0.7, 2.9, and 938 for α3β2 T59K, V111I, and F119Q, respectively. Thus, activity was modestly changed by Ile for Val substitution at β2 nAChR subunit position 111 and changed by >900-fold by Gln substitution for Phe at β2 nAChR subunit position 119.

Circular Dichroism Analysis—Globular LtIA was analyzed by circular dichroism spectroscopy to obtain information on any secondary structural elements present. The peptide was dissolved in 20 mM sodium phosphate buffer, pH 7, and CD spectra were obtained at two different peptide concentrations. Spectra obtained at 52 and 30 μM LtIA overlaid well suggesting that there was no concentration-dependent aggregation. The spectra of all three LtIA peptides, as well as α-conotoxins MII and Vc1.1, are shown in Fig. 6. All peptides show local minima at ~205 nm and a positive band at ~187 nm, which are char-
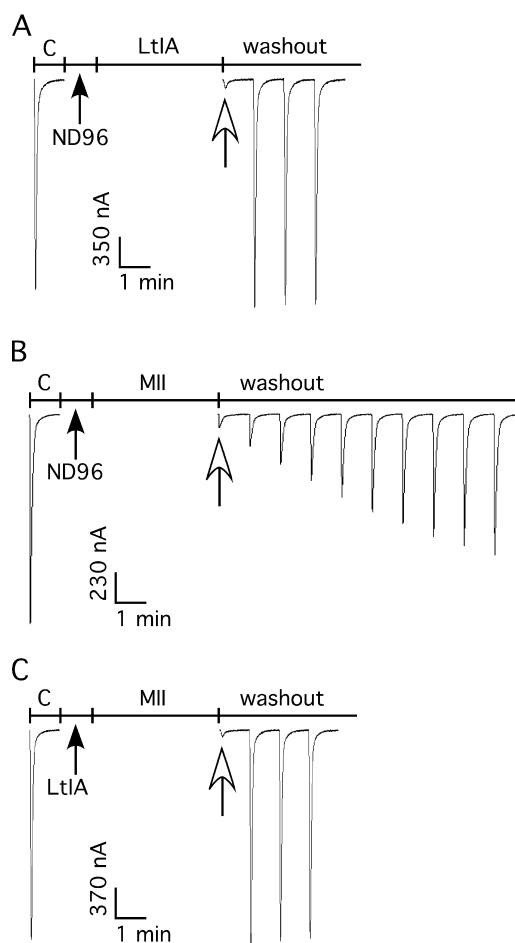

FIGURE 4. **Pre-block of α3β2 nAChRs with α-CTX LtIA prevented the slowly reversible block associated with α-CTX MII.** In each instance, toxin or control solution of ND-96 was applied to α3β2 nAChRs for 1 min followed by a 4-min exposure to toxin or ND-96. *A*, 10 μM α-CTX LtIA was followed by ND-96. *B*, ND-96 was followed by 50 nM α-CTX MII. *C*, 10 μM α-CTX LtIA was followed by 50 nM α-CTX MII.
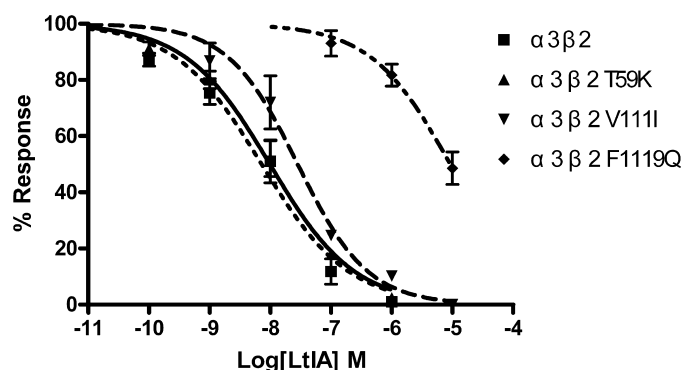
FIGURE 5. **α-CTX LtIA concentration-response on wild type α3β2 nAChRs and their mutant receptors.** All three mutant receptors exhibited similar sensitivity to acetylcholine relative to their wild type α3β2 counterpart. Values are means ± S.E. from 5 to 7 separate oocytes.

acteristic of α-helical structure. Furthermore, minima at 220 nm are more pronounced for LtIA(A4S/A6P), MII, and Vc1.1 consistent with more regular helical structures in these Ser-Xaa-Pro-containing α-conotoxins.

NMR Studies—NMR spectroscopy was employed to further analyze the structure of LtIA. A series of NH-NH_{i+1},

TABLE 3

IC$_{50}$ and Hill slope values for block of rat $\alpha3\beta2$ nAChRs mutants by α-CTX LtIA

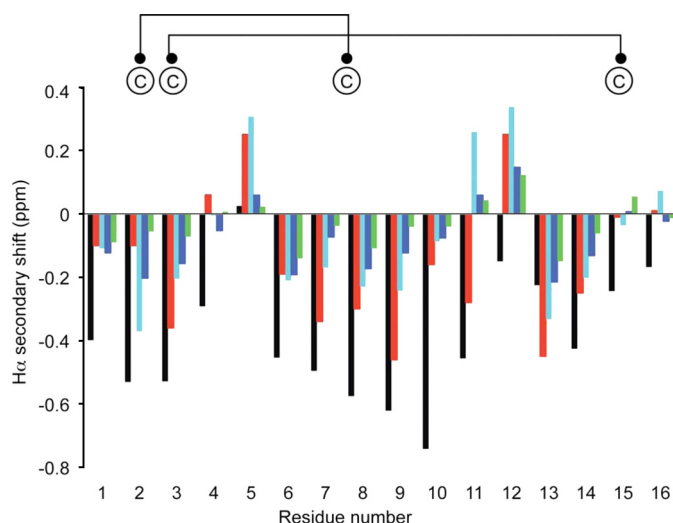| Subtypes	IC$_{50}$[a]	Ratio[b]	Hill slope
	nM		
$\alpha3\beta2$	9.79 (7.3–13.2)	1	0.63 (0.52–0.73)
$\alpha3\beta2$(T59K)	7.2 (4.8–10.7)	0.7	0.61 (0.47–0.75)
$\alpha3\beta2$(V111I)	28.2 (19–42)	2.9	0.76 (0.55–0.96)
$\alpha3\beta2$(F119Q)	9190 (5500–15,500)	939	0.67 (0.41–0.92)

[a] Numbers in parentheses are 95% confidence intervals.
[b] Ratio of nAChR subtype IC$_{50}$/$\alpha3\beta2$ IC$_{50}$.
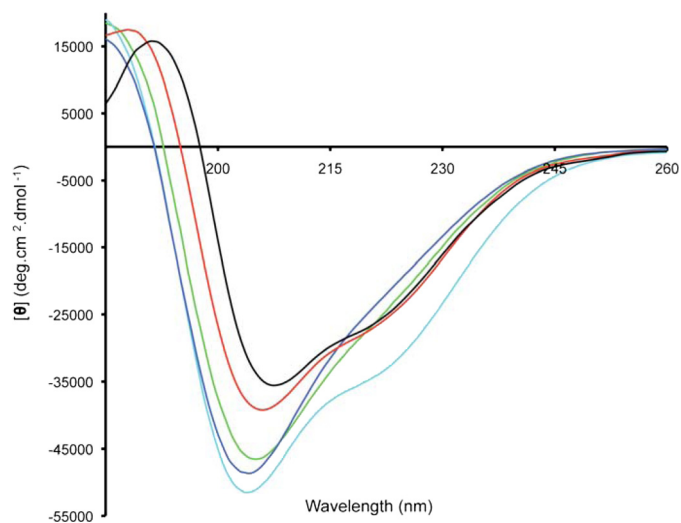
FIGURE 6. **CD spectra of LtIA globular isomer (*green*), (A4S/A6P) (*cyan*), LtIA(A4S) (*blue*), MII (*red*), and Vc1. 1 (*black*).** Spectra were recorded with concentrations of 30–50 μM.

FIGURE 7. **Secondary Hα NMR chemical shifts for LtIA (*green bars*), LtIA(A4S) (*blue*), LtIA(A4S/A6P) (*cyan bars*), Vc1.1 (*black bars*), and MII (*red bars*).** Secondary shifts were calculated by subtracting the random coil chemical shifts (3) from the measured Hα chemical shifts. The disulfide connectivity is shown on the top of the diagram. Data for Vc1.1 and MII are from Refs. 29 and 37.

Hα-NH$_{i+1}$, and Hβ-NH$_{i+1}$ connectivities obtained from the NOESY spectrum was used in conjunction with cross-peaks in the total correlation spectroscopy spectrum to obtain sequence-specific assignments. Differences between the observed Hα chemical shifts and random coil shifts, referred to as secondary shifts, which are generally characteristic of secondary structure elements (36), were calculated and are shown in Fig. 7. A series of small negative secondary shifts for residues 6–9 suggest that LtIA has a propensity for helical structure but is not as well structured as Vc1.1 or MII (29, 37), consistent with the findings from the CD spectral data. NMR spectra for LtIA at 280 K were consistent with those observed at higher temperatures. The double mutant of LtIA containing the Ser-Xaa-Pro motif has secondary shifts for residues 6–9 that are more negative than the wild type LtIA, indicating that the helical structure is stabilized in the central portion of this mutant (Fig. 7). Interestingly, LtIA(A4S) appears to have a lower helical propensity than the wild type peptide, indicating that the proline is important for stabilization of the helix.

The apparently less well defined structure of LtIA relative to most α-conotoxins may explain the relative lack of nuclear Overhauser effects in the NOESY spectrum. Given this lack of nuclear Overhauser effects, no attempt was made to formally calculate a three-dimensional structure using restrained molecular dynamics as has been done for other conotoxins. Thus, the functional and structural studies show that LtIA binds to the $\alpha3\beta2$ nAChR subtype despite possessing a less defined two-turn helical motif. This is an interesting observa-

tion as the helical region has been implicated as important for the activity of other α-conotoxins such as MII, GIC, PIA, and BuIA, which also bind to this receptor subtype (38).

Molecular Modeling of $\alpha3\beta2$ nAChR and Docking Simulation of α-CTX LtIA and MII—Homology modeling was used to study structure-function relationships of LtIA in the absence of experimental three-dimensional structures. We generated structural models for the extracellular domain of the $\alpha3\beta2$ nAChR using the co-crystal structures of $\alpha1$ nAChR-α-bungarotoxin (21) and of α-CTX LtIA and analogs using AChBP-TxIA(A10L) (25) as templates. The docking simulation of α-CTX LtIA with the $\alpha3\beta2$ nAChR model predicted a novel binding mode (Fig. 8), with only the N terminus of LtIA found to overlap with the C terminus of α-CTX TxIA(A10L) (25), ImI (39), or PnIA(A10L/D14K) (38) in AChBP crystal structures. With respect to the TxIA(A10L) complex, α-CTX LtIA adopts an orientation that is rotated 180° around N and C termini along the *y* axis, with its α-helical backbone facing out the binding pocket of the $\alpha3\beta2$ nAChR. The interface of α-CTX LtIA and the $\beta2$ subunit is characterized by two hydrogen bonds between $\beta2$-Gln-34 and LtIA-His-12, $\beta2$-Lys-79, LtIA-Glu-14, Leu-15, and/or Cys-16, and a strong hydrophobic interaction between LtIA-Leu-15 and $\beta2$-Phe-119 (Fig. 8*B* and Table 4). This hydrophobic interaction induced a significant re-orientation of the LtIA-Leu-15 side chain upon energy minimization of the docked structure, highlighting the importance of $\beta2$-Phe-119 in coordinating LtIA and further implicating its role in stabilizing the conformation of $\alpha3\beta2$-LtIA complex. The unique orientation of α-CTX LtIA is further sustained by Arg-5, which is likely to form hydrogen bonds with Ser-38, Ser-168, and Asp-171 from the $\beta2$ F-loop (Fig. 8*C* and Table 4), an interaction that is not seen in any of the previously described α-CTX complexes. This unusual anchor interaction of LtIA-Arg-5 with the $\beta2$ F-loop appears to prevent LtIA from binding deeper into the binding pocket. This shallow binding mode of LtIA supports its fast k_{off} value.
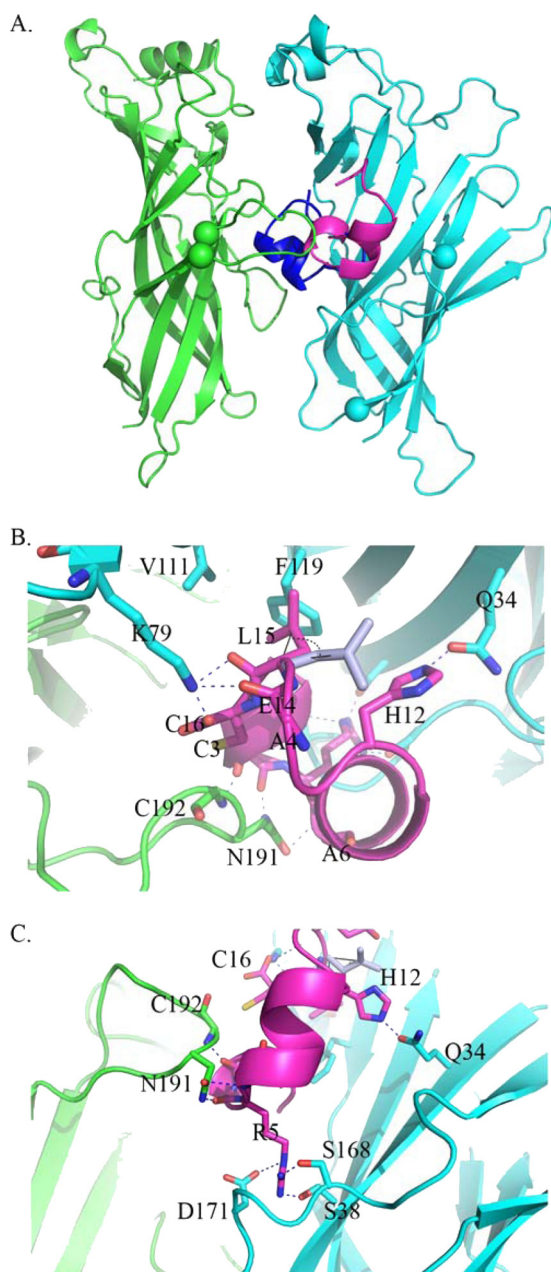
FIGURE 8. Homology modeling and docking simulations for α3β2 (*green/cyan*), LtIA (*magenta*), and MII (*blue*). The interacting residues are presented as *sticks,* and the potential hydrogen bonds are indicated by *blue dashed lines*. C-loop and F-loop are located between the two *green* and two *cyan spheres,* respectively. The superposition of LtIA and MII (*A*) reveals a novel binding mode for LtIA that partially overlaps with that of MII. A noteworthy finding (*B*) in the LtIA binding is that LtIA-Leu-15 side chain swings to form an energetically favorable hydrophobic interaction with β2-Phe-119 after energy minimization. *C,* most prominent interaction of LtIA binding is formed between LtIA-Arg-5 and the β2 F-loop, which acts as an anchor, preventing it from binding deeper into the active site as seen in other α-CTX complexes.

Mutation of the β2 Subunit and LtIA—The LtIA/receptor modeling analysis (assuming a helical structure for bound toxin) predicted that LtIA interacts with nAChR subunit β2-Gln-34 and Lys-79. To experimentally examine these predictions, the β2 subunit was mutated to express α3β2,Q34A and α3β2,K79A in oocytes for assessment of the functional block by LtIA. The β2 subunit Gln to Ala mutation reduced

TABLE 4

Potential hydrogen bonds and hydrophobic interactions between LtIA and α3β2

α3β2 nAChR	LtIA	Distance
		Å
Potential hydrogen bonds		
β2_K79_NZ	Glu-14_O	2.8[a]
β2_K79_NZ	Leu-15_O	2.5[a]
β2_K79_NZ	Cys-16_OXT	1.6[a]
β2_D171_OD2	Arg-5_NE	2.8
β2_S168_OG	Arg-5_NH1	1.8
β2_S38_OG	Arg-5_NH2	1.9
β2_Q34_OE1	His-12_NE2	2.0
α3_C192_N	Cys-3_O	1.9
α3_N191_ND2	Ala-4_O	1.8
α3_N191_OD1	Ala-6_N	2.7
Hydrophobic interactions		
β2_V111	Leu-15	~4.5
β2_F119	Leu-15	~3

[a] The possible H bonds (the closer interaction most likely dominates) are shown.

TABLE 5

IC$_{50}$ values of native and mutant LtIA on native and mutant nAChRs

Numbers are IC$_{50}$ values in nanomolar. Numbers in parentheses indicate 95% confidence intervals.

Peptide	α3β2	α3β2, Q34A	α3β2, K79A
LtIA	9.79 (7.3–13.2)	35.7 (19.7–64.4)	195 (121–315)
LtIA(A4S)	29.1 (20.7–40.8)	87.3 (48.1–158)	73.4 (26.7–202)
LtIA(A4S/A6P)	23.1 (17.3–30.9)	142 (57.0–352)	25.4 (11.8–54.8)

LtIA potency by ~3.5-fold, whereas the Lys to Ala mutation reduced potency by 20-fold, supporting the predictions of the model (see Fig. 8 and Table 5). We next created toxin mutations to examine the effect the Ala-Arg-Ala sequence of LtIA that replaces the highly conserved Ser-Xaa-Pro motif of other α-conotoxins LtIA, A4S, and LtIA(A4S/A6P). The mutant peptides were then tested on wild type and α3β2, Q34A, and α3β2, K79A mutant receptors Results are shown in Fig. 9, *B* and *C,* and Table 5. In contrast to the native LtIA, the double mutant LtIA, which contains the highly conserved Ser-Xaa-Pro of other conotoxins, does not appear to interact with β2-Lys-79.

Interestingly, the conserved Ser-Xaa-Pro motif is replaced with Ala-Arg-Ala in LtIA, where both Ala main chains form hydrogen bonds with Asn-191 from the α3 C-loop (Fig. 8C). The Ala substitutions seem to be essential for binding in the traditional orientation as Ser and Pro at positions 4 and 6, respectively, may contribute to a loss of hydrogen bonding and a resulting steric clash with α3-Asn-191. To confirm this hypothesis, we created homology models for LtIA(A4S) and LtIA(A4S/A6P) using TxIA(A10L) as the template and performed docking simulations to the α3β2 model (Fig 10). In contrast to the native LtIA, both analogs exhibited different binding orientations and lost the intermolecular interactions via Arg-5 and from β2-Lys-79, and yet they retained interactions with β2-Gln-34. This explains why the β2-K79A does not have significant impact to both analogs compared with that with β2-Q34A (Table 5). Furthermore, an additional main chain-main chain interaction between two highly conserved residues, LtIA-Cys-3 and α3-Cys-192, was also identified. A docking model of α-conotoxin MII bound to the α3β2 nAChR was also constructed. Comparison of MII and LtIA binding revealed that the C terminus of MII overlapped the N terminus of LtIA, suggesting LtIA would be a competitive inhibitor of MII binding consistent with our experimental findings (Fig. 4).
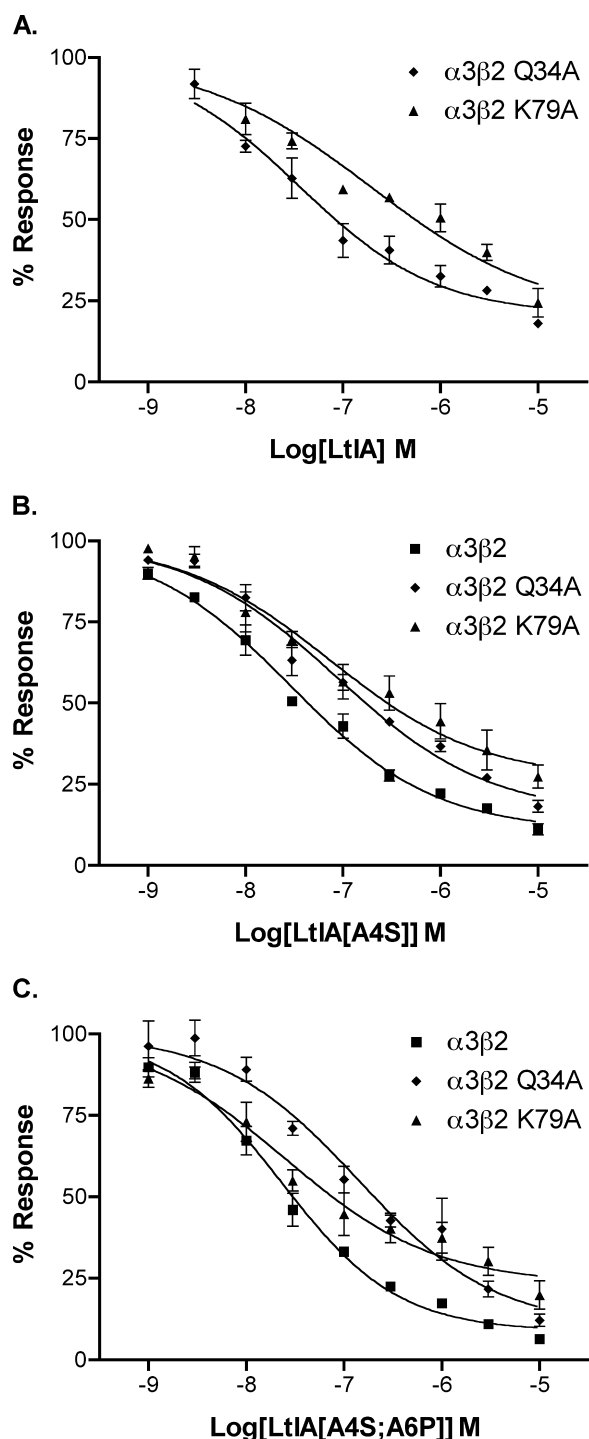
FIGURE 9. **Concentration response of LtIA and LtIA analogs.** Each α-cono-toxin was tested on nAChRs expressed in *Xenopus* oocytes including α3β2 (see Fig. 5 for LtIA), α3β2 with β2 Gln-34 mutated to Ala, and α3β2 with β2 Lys-79 mutated to Ala. *A*, LtIA; *B*, LtIA with Ala-4 mutated to Ser; *C*, LtIA with Ala-4 mutated to Ser and Ala-6 mutated to Pro. Results are summarized in Table 5. Values are mean ± S.E. from 3 to 4 separate oocytes.

DISCUSSION

This study describes the synthesis, pharmacological characterization, structure determination, and receptor interactions of the first α-conotoxin from *C. litteratus*. The peptide, α-CTX LtIA, is highly unusual in that it lacks the conserved Ser-Xaa-Pro motif found in the first Cys loop of all previously reported

α4/7 conotoxins that target neuronal nAChRs (see Table 1). In LtIA, Ala residues replace these conserved Ser and Pro residues found in other conotoxins. Interestingly, substitution of Ala for Ser-4 in synthetic analogs of another potent α4/7 conotoxin, α-CTX MII (see Table 1), shifts selectivity to favor binding to α6/α3β2β3 *versus* α3β2 nAChRs (39, 40). In contrast, LtIA is more potent on α3β2 than α6/α3β2β3 nAChRs (Table 2). In addition, whereas substitution of Ala for Pro in MII dramatically reduces activity at α3β2 nAChRs by 2000-fold (40), α-CTX LtIA has high affinity for α3β2 nAChRs (450-fold higher than the MII (P6A) analog). Thus, the structural and functional studies on LtIA reported here provide a foundation for important mechanistic insights into the interactions of the α-conotoxin class of toxins with nAChRs.

Given the divergent results between α-CTX LtIA and α-CTX MII, we examined whether the two peptides might overlap in their respective binding sites. Both α-CTX LtIA and α-CTX MII potently block α3β2 nAChRs (Figs. 2 and 3); however, α-CTX LtIA differs from α-CTX MII in that the former has a relatively fast off-rate. We utilized this finding to perform a competition experiment to assess whether pre-block of the α3β2 nAChR with a high concentration of α-CTX LtIA could prevent block by subsequent addition of α-CTX MII. The outcome was assessed by measurement of the kinetics of recovery from toxin block. Pre-application of α-CTX LtIA followed by application of α-CTX MII resulted in block of the nAChR with rapid recovery upon toxin washout. This profile is similar to that seen with a block by α-CTX LtIA alone, although not to block by α-CTX MII alone, thus supporting the notion that the two peptides have overlapping binding sites (Fig. 4).

To more rigorously examine the nAChR-binding site, we exploited the different binding selectivity of α-CTX LtIA for α3β2 *versus* α3β4 nAChRs. α-CTX LtIA blocks α3β4 nAChRs with an IC_{50} value that is >1000 higher than that of α3β2 nAChRs. Although there is no NMR or crystal structure of the α3β2 nAChR, the structure of the molluscan AChBP serves as a surrogate (22). The AChBP is a homolog of the extracellular ligand-binding domain of the nAChR, and the AChBP crystal structure sheds significant light on the three-dimensional structure of the ACh-binding site. Furthermore, α-conotoxins have been co-crystallized with the AChBP (41, 42), providing insight into their binding modes. The highly conserved first Cys loop of the α-conotoxins contains a small α-helix important for AChBP and nAChR binding. Thus, the unusual first Cys loop of α-CTX LtIA is of significant interest. Molecular surface analysis and modeling of the α3β2 nAChR and docking of previously characterized α-conotoxins provide evidence of a small cleft above the nAChR β2 subunit β9β10 hairpin as a site for α-conotoxin binding (15). Residues that rim this cleft include Thr-59, Val-111, and Phe-119 (16). Mutation of the nAChR β2 subunit Thr-59 to Lys has a 4-fold effect on α-CTX-MII block (43) and substantially affects the kinetics of block by α-CTX BuIA (44). However, Ala substitution of Val-111 and Ala replacement of Phe-119 have little or no effect on the IC_{50} value of α-CTX MII (16). In contrast, although nAChR β2 subunit mutations T59K and V111I had no effect or a small effect (2.9-fold for V111I) on α-CTX LtIA binding, the F119Q mutation reduced LtIA block by over 900-fold (Fig. 4 and Table 3). Thus,
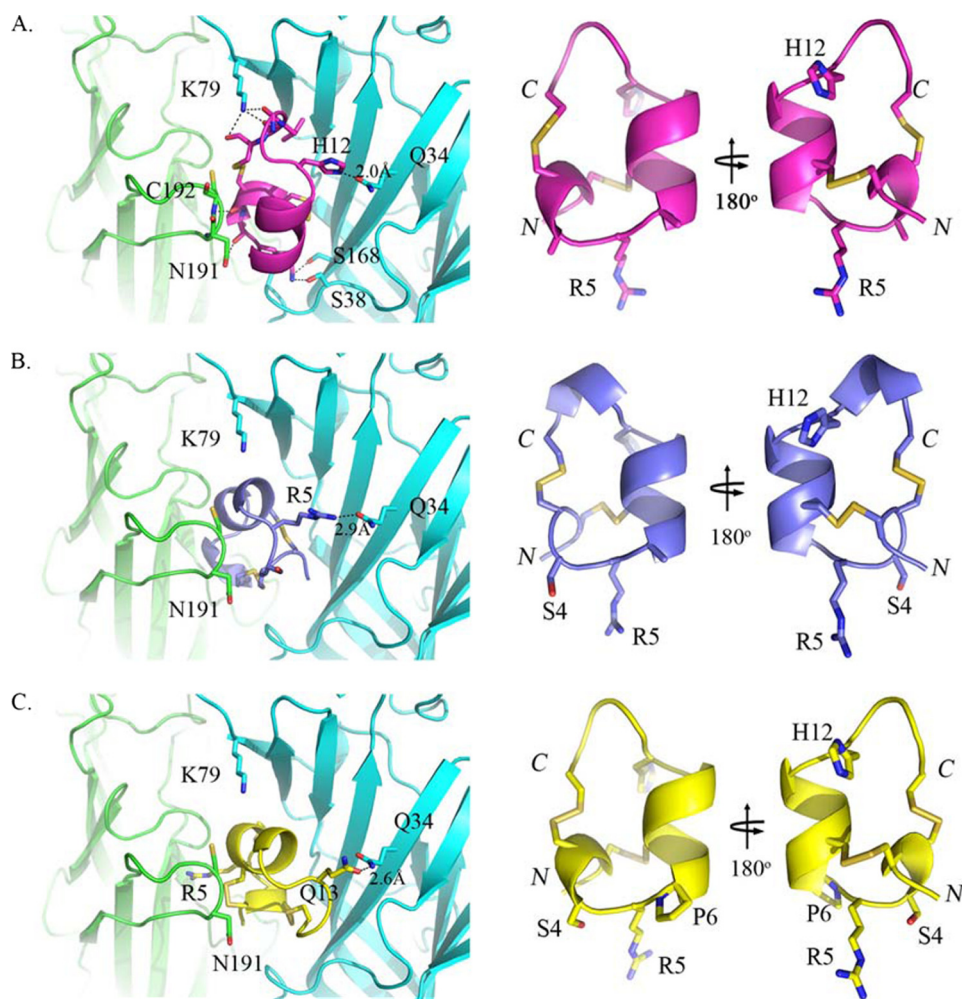
FIGURE 10. **Homology models (*right panel*) and docking simulations (*left panel*) for LtIA (*magenta*) and its analogs LtIA(A4S) (*marine blue*) and LtIA(A4S/A6P) (*yellow*) to α3β2.** The homology models are shown in the identical orientation with the N and C termini labeled in *italic*. The docking complexes on the *left panel* are also presented in the same orientation with key interacting residues shown as *sticks* and the potential hydrogen bonds indicated as *black dashed lines* with distances (Å) labeled. The docking complexes of both LtIA analogs (*B* and *C, left panel*) showed loss of interactions via LtIA-Arg-5 and β2-Lys-79 and rearrangements of hydrogen bonds with β2-Gln-34 compared with that with LtIA (*A, left panel*). The superposition of all three peptides showed no significant alteration in the backbone (root mean square of <0.5 Å), and thus the differences in binding orientation might be due to the steric clash with α3-Asn-191 observed in modeling when A6 was mutated to Pro and a slight shift of α-helix (*B; right panel*) from the N to C termini when A4 was mutated to Ser alone.

lization of the helical structure in the central portion of the peptide when the Ser and Pro residues are introduced (LtIA(A4S/A6P)). The helical propensity of LtIA suggests that it might be able to adopt a well defined helical conformation on receptor binding. Modeling assumed a helical conformation for the peptides and predicted interaction with nAChR β2 subunit residues Gln-34 and Lys-79. Mutation of these receptor residues decreased potency of LtIA consistent with the model. Peptide analogs of LtIA were also synthesized to introduce the Pro and/or Ser residues found in other α-conotoxins (Table 1). Interestingly, the doubly substituted LtIA(A4S/A6P) no longer showed a drop in potency at the α3β2-Lys-79 mutant (Table 5). Thus, although these findings do not prove LtIA adopts a helical conformation when bound, they are consistent with the atypical α-conotoxin LtIA having a distinct binding interaction at α3β2 nAChRs. Although conotoxins are generally regarded as rather rigid peptides, precedent exists for multiple conformations for the globular isomer of other conotoxins, as exemplified for the 4/4 α-conotoxin BuIA (45). Without the conserved Ser-Xaa-Pro motif, it appears that the 4/7 conotoxin framework becomes more flexible, thus providing new opportunities for tuning α-conotoxin selectivity.

Molecular modeling of the α3β2 nAChR and docking simulation also

although the mutation of the nAChR β2 subunit Phe-119 did not affect the IC_{50} value of block by MII, suggesting that MII does not have close interactions with Phe-119, changing Phe-119 to the Gln present in the homologous position of the nAChR β4 subunit dramatically affected block by α-CTX LtIA. These results are consistent with the 3 orders of magnitude higher IC_{50} value of α-CTX LtIA for α3β4 *versus* α3β2 nAChRs (Fig. 3 and Table 2).

Analysis of LtIA by CD and NMR spectroscopy suggested that it has a helical propensity characteristic of most other α-conotoxins, albeit less prominently than Ser-Xaa-Pro containing α-conotoxins. It seems likely that LtIA is relatively flexible in solution, a suggestion supported by the lack of classic helical nuclear Overhauser effects in the NOESY spectrum. Such flexibility is consistent with the absence of the conserved Ser and Pro residues that likely have a structure-defining role in other α-conotoxins. This suggestion is supported by the stabi-

suggested that the binding site of LtIA partially overlaps with that of other 4/7 α-CTXs (Fig. 8*A*) consistent with experimental findings (Fig. 4). This novel binding mode may be driven by several unique interactions that appear to explain LtIA-β2 specificity. The most prominent is the anchor interaction between LtIA-Arg-5 and the β2 F-loop, which is believed to be the key determinant for this shallow binding mode (Fig. 8*C*). Sequence analysis shows no conservation in the F-loop, indicating that this interaction is exclusive to the β2 subunit. Another obvious feature is an energetically favorable hydrophobic interaction between LtIA-Leu-15 and β2-Phe-119, which is achieved by re-orientation of LtIA-Leu-15 side chain after energy minimization. This finding is in agreement with our site-directed mutagenesis data that show a 900-fold increase in the IC_{50} value of LtIA when the hydrophobic interaction is disrupted by β2-F119Q (Fig. 5). In contrast, Val-111 and Thr-59 are >4 and >5 Å distant from LtIA, respectively, suggesting a

weak or no interaction with LtIA, again consistent with our mutagenesis data. In the case of MII, although it is located in a close proximity to Phe-119, Val-111, and Thr-59, only Van der Waals interactions are observed. Furthermore, Ala residues in LtIA that replace the conserved Ser-Xaa-Pro motif allow the accommodation of the α3-Asn-191 side chain and potentially allow the formation of two new hydrogen bonds (Fig. 8*C*). The distinctive binding modes of LtIA(A4S) and LtIA(A4S/A6P) to α3β2 (Fig 10) and the functional studies (Fig. 9 and Table 5) highlight the role of the Ser-Xaa-Pro motif in establishing the binding mode of previously studied α-conotoxins. Intermolecular complementarity between ligand and receptor are essential for ligand binding. As hydrophobic interactions in the active site of nAChR have been postulated as the dominant contributors to α-CTX binding (40, 46), we anticipate that the decrease in hydrophobicity of LtIA due to Ala substitutions may be another key factor for this novel binding mode. Other interactions identified in our docking simulations, especially the interactions distributed from the α3 C-loop, are believed to be involved only in orienting LtIA to the correct position for binding. As most of the ligand-receptor interactions to LtIA appear to arise from the β2 subunit, it is suggested that the ligand selectivity of LtIA for the α3β2 nAChR is determined by the β2 subunit.

In summary, α-CTX LtIA is a novel α-conotoxin that potently blocks α3β2 nAChRs. Structural analysis indicates that the lack of Ser and Pro in the first loop results in a flexible structure that still retains elements of helicity in the solution. Although the bound LtIA structure remains undefined, the profound effect on the block by Gln-34, Lys-79, and Phe-119 mutations in β2 reveals that LtIA binds in a mode that is distinctly different from previously characterized α-conotoxins.

REFERENCES

1. Lester, H. A., Dibas, M. I., Dahan, D. S., Leite, J. F., and Dougherty, D. A. (2004) *Trends Neurosci.* **27,** 329–336
2. Wonnacott, S., Barik, J., Dickinson, J., and Jones, I. W. (2006) *J. Mol. Neurosci.* **30,** 137–140
3. Dani, J. A., and Bertrand, D. (2007) *Annu. Rev. Pharmacol. Toxicol.* **47,** 699–729
4. Gotti, C., Zoli, M., and Clementi, F. (2006) *Trends Pharmacol. Sci.* **27,** 482–491
5. Gotti, C., Riganti, L., Vailati, S., and Clementi, F. (2006) *Curr. Pharm. Des.* **12,** 407–428
6. Olivera, B. M., Quik, M., Vincler, M., and McIntosh, J. M. (2008) *Channels* **2,** 143–152
7. Armishaw, C. J., and Alewood, P. F. (2005) *Curr. Protein Pept. Sci.* **6,** 221–240
8. Craik, D. J., and Adams, D. J. (2007) *ACS Chem. Biol.* **2,** 457–468
9. Zhangsun, D., Luo, S., Wu, Y., Zhu, X., Hu, Y., and Xie, L. (2006) *Chem. Biol. Drug Des.* **68,** 256–265
10. Luo, S., Zhangsun, D., Zhang, B., Chen, X., and Feng, J. (2006) *Peptides* **27,** 2640–2646
11. Terlau, H., and Olivera, B. M. (2004) *Physiol. Rev.* **84,** 41–68
12. Olivera, B. M., and Teichert R. W. (2007) *Mol. Interv.* **7,** 251–260
13. Dutertre, S., and Lewis, R. J. (2004) *Eur. J. Biochem.* **271,** 2327–2334
14. Ellison, M., and Olivera, B. M. (2007) *Chem. Rec.* **7,** 341–353
15. Dutertre, S., Nicke, A., Tyndall, J. D., and Lewis, R. J. (2004) *J. Mol. Recognit.* **17,** 339–347
16. Dutertre, S., Nicke, A., and Lewis, R. J. (2005) *J. Biol. Chem.* **280,** 30460–30468
17. Luo, S., Zhangsun, D., Zhang, B., Quan, Y., and Wu, Y. (2006) *J. Pept. Sci.* **12,** 693–704
18. Peng, C., Han, Y., Sanders, T., Chew, G., Liu, J., Hawrot, E., Chi, C., and Wang, C. (2008) *Peptides* **29,** 1700–1707
19. Dowell, C., Olivera, B. M., Garrett, J. E., Staheli, S. T., Watkins, M., Kuryatov, A., Yoshikami, D., Lindstrom, J. M., and McIntosh, J. M. (2003) *J. Neurosci.* **23,** 8445–8452
20. Cartier, G. E., Yoshikami, D., Gray, W. R., Luo, S., Olivera, B. M., and McIntosh, J. M. (1996) *J. Biol. Chem.* **271,** 7522–7528
21. Dellisanti, C. D., Yao, Y., Stroud, J. C., Wang, Z. Z., and Chen, L. (2007) *Nat. Neurosci.* **10,** 953–962
22. Brejc, K., van Dijk, W. J., Klaassen, R. V., Schuurmans, M., van Der Oost, J., Smit, A. B., and Sixma, T. K. (2001) *Nature* **411,** 269–276
23. Fiser, A., and Sali, A. (2003) *Methods Enzymol.* **374,** 461–491
24. Altschul, S. F., Gish, W., Miller, W., Myers, E. W., and Lipman, D. J. (1990) *J. Mol. Biol.* **215,** 403–410
25. Dutertre, S., Ulens, C., Büttner, R., Fish, A., van Elk, R., Kendel, Y., Hopping, G., Alewood, P. F., Schroeder, C., Nicke, A., Smit, A. B., Sixma, T. K., and Lewis, R. J. (2007) *EMBO J.* **26,** 3858–3867
26. Larkin, M. A., Blackshields, G., Brown, N. P., Chenna, R., McGettigan, P. A., McWilliam, H., Valentin, F., Wallace, I. M., Wilm, A., Lopez, R., Thompson, J. D., Gibson, T. J., and Higgins, D. G. (2007) *Bioinformatics* **23,** 2947–2948
27. Bowie, J. U., Lüthy, R., and Eisenberg, D. (1991) *Science* **253,** 164–170
28. Laskowski, R. A., Watson, J. D., and Thornton, J. M. (2005) *Nucleic Acids Res.* **33,** W89–W93
29. Hill, J. M., Oomen, C. J., Miranda, L. P., Bingham, J. P., Alewood, P. F., and Craik, D. J. (1998) *Biochemistry* **37,** 15621–15630
30. Bourne, Y., Talley, T. T., Hansen, S. B., Taylor, P., and Marchot, P. (2005) *EMBO J.* **24,** 1512–1522
31. Ritchie, D. W., and Kemp, G. J. (2000) *Proteins Struct. Funct. Genet.* **39,** 178–194
32. Vriend, G. (1990) *J. Mol. Graph.* **8,** 52–56, 29
33. Gehrmann, J., Alewood, P. F., and Craik, D. J. (1998) *J. Mol. Biol.* **278,** 401–415
34. Schnölzer, M., Alewood, P., Jones, A., Alewood, D., and Kent, S. B. (1992) *Int. J. Pept. Protein Res.* **40,** 180–193
35. McIntosh, J. M., Azam, L., Staheli, S., Dowell, C., Lindstrom, J. M., Kuryatov, A., Garrett, J. E., Marks, M. J., and Whiteaker, P. (2004) *Mol. Pharmacol.* **65,** 944–952
36. Sönnichsen, F. D., Van Eyk, J. E., Hodges, R. S., and Sykes, B. D. (1992) *Biochemistry* **31,** 8790–8798
37. Clark, R. J., Fischer, H., Nevin, S. T., Adams, D. J., and Craik, D. J. (2006) *J. Biol. Chem.* **281,** 23254–23263
38. Wishart, D. S., Sykes, B. D., and Richards, F. M. (1992) *Biochemistry* **31,** 1647–1651
39. Ulens, C., Hogg, R. C., Celie, P. H., Bertrand, D., Tsetlin, V., Smit, A. B., and Sixma, T. K. (2006) *Proc. Natl. Acad. Sci. U.S.A.* **103,** 3615–3620
40. Celie, P. H., Kasheverov, I. E., Mordvintsev, D. Y., Hogg, R. C., van Nierop, P., van Elk, R., van Rossum-Fikkert, S. E., Zhmak, M. N., Bertrand, D., Tsetlin, V., Sixma, T. K., and Smit, A. B. (2005) *Nat. Struct. Mol. Biol.* **12,** 582–588
41. Hansen, S. B., Sulzenbacher, G., Huxford, T., Marchot, P., Taylor, P., and Bourne, Y. (2005) *EMBO J.* **24,** 3635–3646
42. Celie, P. H., Klaassen, R. V., van Rossum-Fikkert, S. E., van Elk, R., van Nierop, P., Smit, A. B., and Sixma, T. K. (2005) *J. Biol. Chem.* **280,** 26457–26466
43. Azam, L., Yoshikami, D., and McIntosh, J. M. (2008) *J. Biol. Chem.* **283,** 11625–11632
44. Shiembob, D. L., Roberts, R. L., Luetje, C. W., and McIntosh, J. M. (2006) *Biochemistry* **45,** 11200–11207
45. Jin, A. H., Brandstaetter, H., Nevin, S. T., Tan, C. C., Clark, R. J., Adams, D. J., Alewood, P. F., Craik, D. J., and Daly, N. L. (2007) *BMC Struct. Biol.* **7,** 28
46. Quiram, P. A., McIntosh, J. M., and Sine, S. M. (2000) *J. Biol. Chem.* **275,**

4889 – 4896

47. McIntosh, J. M., Dowell, C., Watkins, M., Garrett, J. E., Yoshikami, D., and Olivera, B. M. (2002) *J. Biol. Chem.* **277,** 33610 – 33615

48. Vincler, M., Wittenauer, S., Parker, R., Ellison, M., Olivera, B. M., and McIntosh, J. M. (2006) *Proc. Natl. Acad. Sci. U.S.A.* **103,** 17880 – 17884

49. Sandall, D. W., Satkunanathan, N., Keays, D. A., Polidano, M. A., Liping, X., Pham, V., Down, J. G., Khalil, Z., Livett, B. G., and Gayler, K. R. (2003) *Biochemistry* **42,** 6904 – 6911

50. Chi, S. W., Kim, D. H., Olivera, B. M., McIntosh, J. M., and Han, K. H. (2006) *Biochem. Biophys. Res. Commun.* **345,** 248 – 254

51. Luo, S., Nguyen, T. A., Cartier, G. E., Olivera, B. M., Yoshikami, D., and McIntosh, J. M. (1999) *Biochemistry* **38,** 14542 – 14548

52. Loughnan, M. L., Nicke, A., Jones, A., Adams, D. J., Alewood, P. F., and Lewis, R. J. (2004) *J. Med. Chem.* **47,** 1234 – 1241

53. Hogg, R. C., Miranda, L. P., Craik, D. J., Lewis, R. J., Alewood, P. F., and Adams, D. J. (1999) *J. Biol. Chem.* **274,** 36559 – 36564

54. McIntosh, J. M., Plazas, P. V., Watkins, M., Gomez-Casati, M. E., Olivera, B. M., and Elgoyhen, A. B. (2005) *J. Biol. Chem.* **280,** 30107 – 30112

55. Loughnan, M., Bond, T., Atkins, A., Cuevas, J., Adams, D. J., Broxton, N. M., Livett, B. G., Down, J. G., Jones, A., Alewood, P. F., and Lewis, R. J. (1998) *J. Biol. Chem.* **273,** 15667 – 15674

56. Luo, S., Kulak, J. M., Cartier, G. E., Jacobsen, R. B., Yoshikami, D., Olivera, B. M., and McIntosh, J. M. (1998) *J. Neurosci.* **18,** 8571 – 8579

57. López-Vera, E., Aguilar, M. B., Schiavon, E., Marinzi, C., Ortiz, E., Restano, Cassulini, R., Batista, C. V., Possani, L. D., Heimer de la Cotera, E. P., Peri, F., Becerril, B., and Wanke, E. (2007) *FEBS J.* **274,** 3972 – 3985